# A Combined Theoretical and Experimental Study of the Photophysics of Asulam

**ARTICLE** *in* THE JOURNAL OF PHYSICAL CHEMISTRY A · FEBRUARY 2013

Impact Factor: 2.69 · DOI: 10.1021/jp311932z · Source: PubMed



**9 AUTHORS**, INCLUDING:

Cristina Martinez Garcia
University of A Coruña
**7** PUBLICATIONS **168** CITATIONS
SEE PROFILE

Moisés Canle López
University of A Coruña
**124** PUBLICATIONS **1,397** CITATIONS
SEE PROFILE

J. Arturo Santaballa
University of A Coruña
**98** PUBLICATIONS **1,235** CITATIONS
SEE PROFILE

THE JOURNAL OF PHYSICAL CHEMISTRY A

Article

pubs.acs.org/JPCA

# Combined Theoretical and Experimental Study of the Photophysics of Asulam

Angelo Giussani,*[,†] Rosendo Pou-Amérigo,[†] Luis Serrano-Andrés,[†] Antonio Freire-Corbacho,[‡] Cristina Martínez-García,[‡] Mª Isabel Fernández P.,[‡] Mohamed Sarakha,[§] Moisés Canle L.,[‡] and J. Arturo Santaballa*[,‡]

[†]Instituto de Ciencia Molecular, Universitat de Valencia, Ap. 22085, ES-46100 Valencia, Spain

[‡]Departamento de Química Física e Enxeñería Química I, Universidade da Coruña, Rúa da Fraga 10, ES-15008 A Coruña, Spain

[§]Laboratoire de Photochemie Moléculaire et Macromoléculaire, Université Blaise Pascal, UMR CNRS 6505, F-63177 Aubière Cedex, France

Supporting Information

**ABSTRACT:** The photophysics of the neutral molecular form of the herbicide asulam has been described in a joint experimental and theoretical, at the CASPT2 level, study. The unique $\pi \rightarrow \pi^*$ aromatic electronic transition (f, ca. 0.5) shows a weak red-shift as the polarity of the solvent is increased, whereas the fluorescence band undergoes larger red-shifts. Solvatochromic data point to higher dipole moment in the excited state than in the ground state ($\mu_g < \mu_e$). The observed increase in p$K_a$ in the excited state (p$K_a$* − p$K_a$, ca. 3) is consistent with the results of the Kamlet−Abboud−Taft and Catalán et al. multiparametric approaches. Fluorescence quantum yield varies with the solvent, higher in water ($\phi_f$ = 0.16) and lower in methanol and 1-propanol (approx. 0.02). Room temperature fluorescence lifetime in aqueous solution is (1.0 ± 0.2) ns, whereas the phosphorescence lifetime in glassy EtOH at 77 K and the corresponding quantum yield are (1.1 ± 0.1) s and 0.36, respectively. The lack of mirror image symmetry between modified absorption and fluorescence spectra reflects different nuclear configurations in the absorbing and emitting states. The low value measured for the fluorescence quantum yield is justified by an efficient nonradiative decay channel, related with the presence of an easily accessible conical intersection between the initially populated singlet bright $^1(L_a\ \pi\pi^*)$ state and the ground state $(gs/\pi\pi^*)_{CI}$. Along the main decay path of the $^1(L_a\ \pi\pi^*)$ state the system undergoes an internal conversion process that switches part of the population from the bright $^1(L_a\ \pi\pi^*)$ to the dark $^1(L_b\ \pi\pi^*)$ state, which is responsible for the fluorescence. Additionally, singlet−triplet crossing regions have been found, a fact that can explain the phosphorescent emission detected. An intersystem crossing region between the phosphorescent state $^3(L_a\ \pi\pi^*)$ and the ground state has been characterized, which contributes to the nonradiative deactivation of the excitation energy.

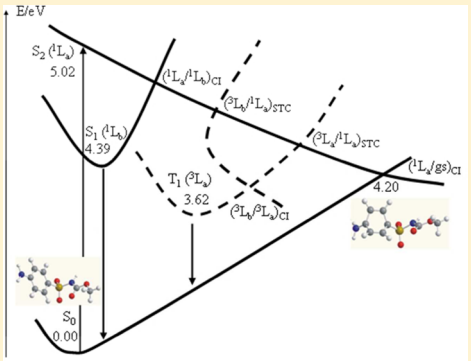


## INTRODUCTION

Soil and groundwater pollution are the major environmental concern for pesticides application; they could either leach and contaminate groundwater or persist on the surface, becoming harmful to microorganisms, plants, and animals.[1] Its persistence in the environment has serious negative consequences for human health and for the equilibrium of ecosystems.[2] During the past decade water treatment technology moved toward advanced oxidation procedures; between them the use of UV-light irradiation has been found highly advantageous for pollutants abatement. Promoting the use of photodisposable chemicals can solve many of the already detected problems. Finding appropriate substances prompts for accurately establishing the photophysical and photochemical properties of the most common pesticides.

Because of its extensive use, herein we focus on asulam, methyl((4-aminophenyl)sulfonyl)carbamate or *N*-(4-aminophenyl)sulfonylcarbamic acid methyl ester (see Figure 1), which was declared not permitted by the Commission Implementing Regulation (EU) No 1045/2011 of 19 October 2011,[3] as well as its sodium salt (trade name Asulox). Asulam, a

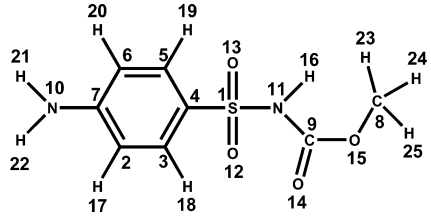

**Figure 1.** Structure and atom numbering of methyl[(4-aminophenyl)-sulfonyl] carbamate (asulam).

**Received:** June 30, 2012
**Revised:** February 11, 2013
**Published:** February 14, 2013

selective systemic herbicide, is used for control of annual and perennial grasses and broad-leaved weeds in spinach, oilseed poppies, alfalfa, some ornamentals, sugar cane, bananas, coffee, tea, cocoa, coconuts, rubber, fruit trees and bushes, and forestry.[4,5] It has been extensively used in the U.K., where many land managers are claiming against the ban on its use, as they lost the main weapon for bracken control. Asulam is extremely mobile and has a strong potential to leach into groundwater or to move through surface water masses. It is highly soluble in water, not volatile, stable in water in the absence of light, and unstable in water and on soil under irradiation.[6] The half-life of aqueous asulam, under typical Central Europe daylight irradiation,[7] is ca. three hours in June, whereas it takes ca. 11 hours in January.[8] Complete mineralization was observed after 30 h of 365 nm irradiation in the presence of aqueous $Fe^{2+}$ ($3 \times 10^{-4}$ M) at pH ca. 3 and under air atmosphere.[6] Asulam photolytic quantum yield was estimated to be 0.18 upon UV light excitation (254−313 nm) at pH = 7 and under air atmosphere. It increased to about 0.57 in deoxygenated solution and decreased to 0.17 in oxygen saturated solution. The photolytic quantum yield reduces to ca. 0.13 when 3 < pH < 5, and ca. 0.02 at pH = 1.5.[8] In spite of asulam being reported as practically nontoxic to freshwater fish, estuarine/marine species, honeybees, and small mammals and posing minimal risk to freshwater invertebrates,[9] the EU report concluded that more tests were needed for a consumer risk assessment on spinach, and that is a high long-term risk to herbivorous and insectivorous birds.[4]

The title molecule is consequently important for different reasons: it has been widely used in agriculture and its controversial ban in the European Union; its particular structure, as this carbamate contains a sulfonyl group linked to an aminophenyl group, which might imply higher electron delocalization and the existence of the neutral and anionic forms in aqueous solution; it could give information about an important class of compounds (the carbamate pesticides); and there are different works pointing to its photodegradation.[68] The last feature is particularly interesting and attractive since the use of photodegradable herbicides would considerably simplify the contamination problems related with the employ of chemical agents in the primary sector of the economy. In order to explore this possibility, a basic requirement would be the knowledge of the main photoresponse of the candidate systems.

In the described context, the present contribution can be framed as a first step toward the comprehension of the photoinduced processes of the largely employed herbicide asulam, whose properties are of interest for its intrinsic importance and in relation with other possible compounds. The aim of the present contribution is to determine the photophysics of the systemic herbicide asulam by means of combined theoretical and experimental methodologies. Experimental measurements on the absorption and emission, both fluorescence and phosphorescence, solvatochromic effects, and multiconfigurational quantum-chemical ab initio CASPT2 calculations on the low-lying singlet and triplet states will be employed to describe and rationalize the main population and photophysical decay pathways on the molecule upon UV irradiation.

Solvent effects on UV−vis absorption spectra can be used to determine the magnitude of the electric dipole moment of solute molecules in electronically excited state and provide useful information about the electronic and geometrical structure of the molecule in its short-lived excited state. Contrary to the case of ground state, there are not many reliable techniques available for the estimation of the dipole moment of electronically excited states; among the existing methods, the most popular ones are based on a linear correlation between the wavenumbers of the absorption and fluorescence maxima ($\bar{\nu}_{a,max}$, $\bar{\nu}_{f,max}$) and solvent polarity functions, usually involving both the static dielectric constant ($\varepsilon$) and the refractive index ($n$) of the medium,[10] i.e., the solvatochromic method. UV−vis absorption and emission spectra of a solute in different solvents can also be used to unravel solvation interactions at the molecular level in terms of multiparameter relationships like those due to Kamlet−Abboud−Taft[11−14] or Catalán et al.[15]

Over the past decade, the CASPT2//CASSCF methodology has been proven to be an efficient and reliable computational tool in order to study the photophysics and photochemistry of medium-size organic molecules. Such method is in fact able to provide a balanced description of the potential energy hypersurfaces of the excited states of a system along different nuclear conformations and, consequently, allowed a coherent description of the deactivation processes that the molecule may undergo after UV absorption. The photoresponse of many basic chromophores have been in fact rationalized on the basis of quantum chemical CASPT2//CASSCF calculation, like, for example, pyrimidine and purine nucleobases,[16,17] other relevant biological systems,[18] and model pesticides.[19]

## EXPERIMENTAL AND COMPUTATIONAL DETAILS

**Experimental Section.** Asulam-methyl[(4-aminophenyl)-sulfonyl] carbamate (purity 96%), purchased from Riedel-de Häen, has been used as received; its purity was checked by high-performance liquid chromatography (HPLC) and nuclear magentic resonance (NMR). Aniline (Aldrich A.C.S reagent) has been further purified by microdistillation under nitrogen atmosphere.

Organic solvents, purchased from Sigma−Aldrich or Merck, all of spectroscopic or HPLC quality, were used as received and did not show any traces of fluorescence. Water has been doubly distilled.

Steady-state UV−vis absorption spectra have been recorded at room temperature on a Beckman DU-70 spectrophotometer with a wavelength accuracy of ±0.1 nm. Fluorescence spectra have been recorded, also at room temperature, using a spectrofluorimeter (Aminco-Bowman Series 2) equipped with a 150 W continuous Xenon lamp. For all spectral measurements Suprasil quartz cells of 1 cm light path were used.

Fluorescence quantum yields ($\phi_f$) have been calculated using the comparative method,[20] with aniline as standard,[21] according to the following equation:

$$\phi_f^i = \phi_f^s \frac{A_s}{A_i} \frac{I_f^i(\lambda)}{I_f^s(\lambda)} \frac{{n_i}^2}{{n_s}^2}$$

where i and s refer to asulam and standard, respectively; $A$ is the absorption at the excitation wavelength (282 nm); $I_f$ stands for the fluorescence intensity, and $n$ represents the refractive index of the solvent. Low concentration has been used (ca. $8.0 \times 10^{-6}$ mol·dm$^{-3}$) ensuring that the approximations involved in the above equation are met.

The demodulation and phase shift measurements of fluorescence lifetimes have been done using a SLM 48000S Multiple Frecuency Lifetime Spectrofluoremeter SIM AMINCO equipped with a 450 W xenon lamp as light source.

Lifetime measurements, in the range 20 ps to 1.58 ms, were performed at different modulation frequencies between 10 kHz to 2 GHz, and the obtained fluorescence lifetime was averaged for all of them.

Phosphorescence spectra were recorded at 77 K in glassy EtOH using a spectrofluorimeter (Aminco-Bowman Series 2) equipped with a 7 W pulsed Xenon lamp, exciting at 282 nm. The phosphorescence decay curves were collected at 404 nm and analyzed according to a first order kinetic model to obtain the phosphorescence decay time ($\tau_P$).

**Computational Section.** The present calculations include CASSCF geometry optimizations, minimum energy paths (MEP), and conical intersection and singlet−triplet crossing searches, followed by multiconfigurational perturbation theory (CASPT2) calculations at the optimized geometries, using a standard zeroth-order Hamiltonian.[22,23] An imaginary level shift of 0.1 au has been employed to prevent the presence of intruder states. Spin−orbit coupling terms and transition dipole moments have also been computed. The final results involve an active space of 6 electrons distributed in 6 orbitals, CASPT2-(6,6)//CASSCF (see Figure SI13 of the Supporting Information). A one-electron basis set of the ANO-S type contracted to S[4s3p1d]/C,N,O[3s2p1d]/H[2s] has been used throughout. The ground state and the Onsager cavity radius, however, used a geometry optimized at the DFT/B3LYP/6-31G(d) level of calculation. MEPs have been built as steepest-descendent paths in which each step required the minimization of the energy on a hyperspherical cross-section of the PEH centered on the initial geometry and characterized by a predefined radius. Conical intersections and singlet−triplet crossings have been computed as minimum energy crossing points (MECP) on the PEH.[24,25] No spatial symmetry restrictions were imposed. More detailed technical aspects of the calculations can be found in the Supporting Information. The calculations reported used the quantum chemical methods implemented in the MOLCAS 7.2 package [26] and the Gaussian 09 suite.[27]

## RESULTS AND DISCUSSION

**A. Steady-State Absorption and Fluorescence Spectra.** Asulam can exist in three forms in aqueous solution (Figure 2), their relative concentration depending on the acidity of the medium.[28]

Room temperature UV−vis absorption and fluorescence spectra of asulam have been measured in different solvents. The electronic (UV−vis) absorption spectra of the molecular form of asulam (**1**) in water, ethanol (Figure 3), and other organic solvents show one intense structureless band with a broad, well-defined peak, with onset at ca. 32 000 $cm^{-1}$ (312.5 nm) and a maximum centered at ca. 37 500 $cm^{-1}$ (344 nm) (Table 1).

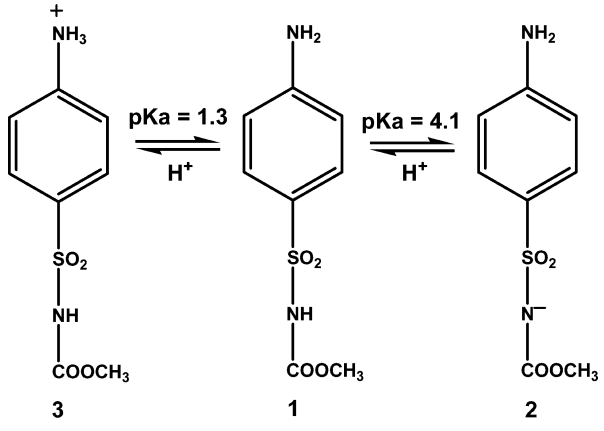


**Figure 2.** Acid−base equilibria of asulam in aqueous solution.

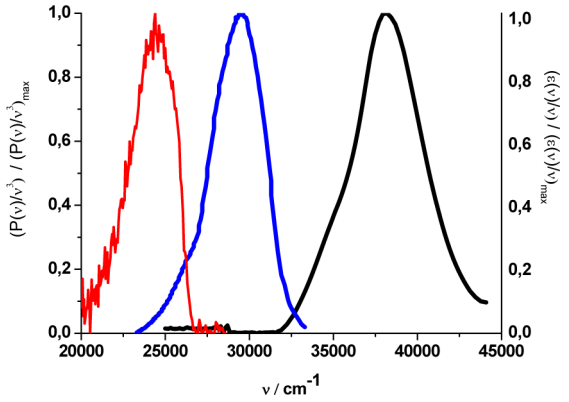


**Figure 3.** Steady-state spectra of ethanolic 16 $\mu$M asulam in its molecular form (**1**). From the left to the right: phosphorescence (ca. 77 K), fluorescence, and UV−vis absorption (ca. 298 K).

**Table 1. Solvent Effects on the Electronic Absorption and Fluorescence Spectral Data of the Molecular Form of Asulam (1)[a]**

| solvent | $\bar{\nu}_{a,max}$ ($cm^{-1}$(nm)) | $\bar{\nu}_{f,max}$ ($cm^{-1}$(nm)) | $\bar{\nu}_{a,max} - \bar{\nu}_{f,max}$ ($cm^{-1}$) |
|---|---|---|---|
| dichloromethane | 37594 (266) | 30864 (324) | 6730 |
| trichloromethane | 37736 (265) | 30864 (324) | 6872 |
| propan-1-ol | 37313 (268) | 29761 (336) | 7552 |
| acetonitrile | 37313 (268) | 30030 (333) | 7283 |
| methanol | 37453 (267) | 29673 (337) | 7780 |
| ethanol | 38197 (262) | 29762 (336) | 8435 |
| ethylene glycol | 36900 (271) | 29761 (336) | 7139 |
| 1,4-dioxane | 37594 (266) | 30211 (331) | 7383 |
| diethyl ether | 37453 (267) | 30487 (328) | 6966 |
| water | 37313 (268) | 29412 (340) | 7901 |

[a] $T \approx 298$ K.

The steady-state absorption spectra of **1** show a relatively small solvent effect on the position and shape of the absorption band (Table 1). Bathochromic shifts were observed as solvent polarity increased, except for ethanol. The corresponding molar absorption coefficient was large, $\varepsilon_{max}$(in $H_2O$) = 16 836 $mol^{-1}\cdot dm^3\cdot cm^{-1}$ at $\lambda_{max}$ = 268 nm. On the basis of all these evidence, the absorption band located in the 270 nm region was attributed to $\pi \rightarrow \pi^*$ aromatic electronic transitions, in agreement with similar observations for aniline.[29]

The intrinsic ability of a molecule to absorb light is often expressed in terms of the oscillator strength for the electronic transition ($f$), which can be determined experimentally by integrating the molar absorptivity over the frequency $\nu$ (in $cm^{-1}$) according to the following equation:[30]

$$f = \frac{4.39 \times 10^{-9}}{n} \int_{\bar{\nu}_2}^{\bar{\nu}_1} \varepsilon(\bar{\nu}) \mathrm{d}\bar{\nu}$$

where the molar absorptivity, $\varepsilon(\bar{\nu})$, has units of $dm^3\cdot mol^{-1}\cdot cm^{-1}$, and the frequency, $\nu$, is expressed in wavenumber ($cm^{-1}$). This integration extends from $\bar{\nu}_1$ to $\bar{\nu}_2$,


dx.doi.org/10.1021/jp311932z | J. Phys. Chem. A 2013, 117, 2125−2137

Table 2. Fluorescence Quantum Yield for Asulam, $\phi_f$, Obtained Using the Comparative Method, Taking Aniline As a Reference ($\lambda_{exc}$ = 282 nm, $T$ = 298 K)

| | | | pH | | | | | |
|---|---|---|---|---|---|---|---|---|
| solvent | | | 3.21 | 6.52 | 7.80 | 9.09 | 10.2 | 10.9 |
| 1,4-dioxane | 0.057 | | | | | | | |
| diethyl ether | 0.099 | | | | | | | |
| methanol | 0.023 | | | | | | | |
| water | 0.155 | 0.032[b] | 0.186 | 0.201 | 0.189 | 0.171 | 0.190 | 0.165 |
| acetonitrile | 0.032 | 0.15[a] | | | | | | |
| propan-1-ol | 0.025 | | | | | | | |

[a]Ref 41. [b]Ref 42.

which are the limits of the band associated with the electronic transition from lower to upper state, and $n$ stands for the refractive index of the solvent. Values of $f$ in water, neutral, and acidic conditions and in ethanol were 0.48 and 0.50, respectively, implying a strong transition.

The best quantitative measure of the transition probability, the transition dipole moment ($\mu_{g\to e}$), has been obtained in terms of the oscillator strength by using the expression[31]

$$\mu_{g\to e} = \sqrt{\frac{3he^2 f}{8\pi^2 m_e c \overline{\nu}_{a,max}}}$$

where $e$ is the elementary charge, $m_e$ the electron mass, $c$ the light speed in vacuum, and $h$ the Planck's constant. Assuming the electronic degeneracies of the lower and upper state are the same, 5.3 D (ethanol) and 5.2 D (water) have been estimated for the transition dipole moment $\mu_{g\to e}$.

Room temperature steady-state fluorescence spectra of the molecular form of asulam (**1**) in some organic solvents is shown in Figure SI1 of the Supporting Information, and the corresponding maxima ($\overline{\nu}_{f,max}$) and Stokes' shifts ($\overline{\nu}_{a,max} - \overline{\nu}_{f,max}$) are compiled in Table 1. Red shifts on the position and shape of the structureless band are observed, larger than for absorption. The amino group plays a role in asulam's fluorescence, as benzenesulphonamide does not show it, but it is present in the closely related sulphanilamide.[32]

The frequency of the electronic 0−0 transition between the ground state and the excited singlet state has been determined from the abscissa corresponding to the intersection point of the modified absorption spectrum, $\varepsilon(\overline{\nu})/\overline{\nu}$ versus $\overline{\nu}$, and the normalized modified fluorescence spectrum, $I_f(\overline{\nu})/\overline{\nu}^3$ versus $\overline{\nu}$,[33] where $\overline{\nu}$ is the wavenumber (in $cm^{-1}$). Similar values have been found for such 0−0 transition in water and ethanol, 307 and 306 nm, respectively. However, the crossing between fluorescence and phosphorescence bands takes place at 380 nm (Figure 3). No mirror image symmetry exists between the absorption and fluorescence spectra (Figure 3), indicating that the geometry of the molecular form of asulam (**1**) in the emitting and absorbing states is not the same.[34,35]

The fluorescence spectra is more sensitive to the nature of the solvents, which points to a larger charge transfer taking place from the amino group to the aromatic ring in the excited state in comparison to the ground state and also to a larger dipole moment in the excited state than for $S_0$. In the case of aniline noticeable solvent-induced shifts in the maximum of fluorescence have been observed,[36] and the Stokes shift between absorption and fluorescence maxima varies with the polarity of the solvent.

The anionic form of asulam (**2**) also shows fluorescence; the corresponding room temperature steady−state fluorescence and absorption spectra are depicted in Figure SI2 of the Supporting Information. In aqueous solution the absorbance maximum of **2** moves to lower wavelength ($\lambda_{max}$ = 256 nm) relative to the neutral form (**1**), its shape and intensity remaining nearly unchanged. The fluorescence spectra of **1** and **2** show an almost coinciding broad band, 3-fold less intense for **1** than for **2**. The coincidence of the fluorescence peaks of the anionic and molecular forms is usually observed in sulfonamides.[37] The p$K_a$ of the excited state can be estimated using the absorption data of the molecular and anionic forms in the Förster's cycle.[38] Thus, the p$K_a$ of the excited state (p$K_a$*) increases 3.1 units, i.e., excited asulam becomes more basic. The same behavior has been reported for sulfonylureas, which show similar acid−base chemistry.[28]

This behavior is opposite to that of aniline, where a decrease of ca. 8 units is observed.[39] The deprotonation leads to a negatively charged species (**2**) for asulam, while aniline becomes neutral.

The phosphorescence spectrum of the molecular form of asulam (**1**) shows a relatively unsymmetrical band with a maximum centered at 405 nm (Figure 3). Phosphorescence of sulfanilamide and some derivatives in the same matrix, and temperature, occurs in the same region (405−420 nm),[37,40] and it can be assigned to a $\pi^* \to \pi$ transition from the lowest triplet state.[37]

*Photophysics.* The measured fluorescence quantum yields in some organic solvents and under different acidity conditions in water for **1** are collected in Table 2. No clear trend is observed with either the polarity of the solvent or the acidity. Aqueous solutions show the highest fluorescence quantum yield, which implies that the presence of water induces a decrease in the decay rate for the nonradiative channels.

Other than water, the higher quantum yields of **1** are observed in diethyl ether and dioxan. The reason for the value observed in dioxane was justified by Forbes for aniline, which shows similar results.[43] He suggested the formation of an aniline−dioxan interaction complex that enhances $\phi_f$ (based on a higher degree of $e^-$-transfer from the N to the ring that allows a higher population on the excited state). A similar explanation should be feasible for ethyl ether.

In the case of water, Blais and Gauthier[44] obtained for aniline a decrease of quantum yield with respect to organic solvents not containing hydroxyl groups; the interaction between water and the lone electron pair of the amino nitrogen, forming a 1:1 complex, lead to such decrease. However, in the case of asulam, the quantum yield in water is the largest (Table 2), a possible explanation being the presence of the electron-withdrawing sufonyl group that may sensibly reduce electron density around the amino group, hence weakening the interaction between water and the unshared electron pair of the amino nitrogen, as

compared with aniline (Figure 4), the net effect being a larger fluorescence quantum yield.

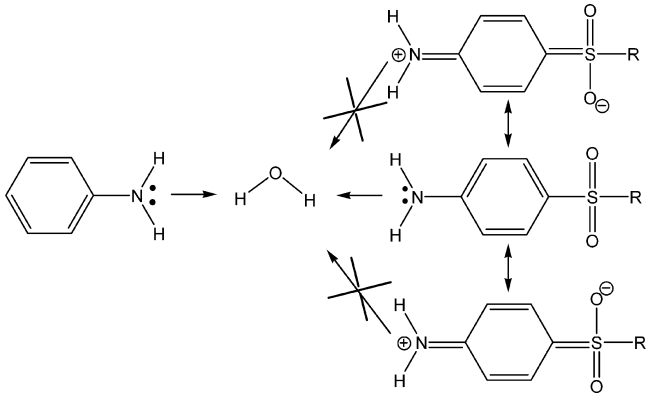

**Figure 4.** Differential interactions between water and the lone electron pair of the amino nitrogen in aniline and asulam.

Fluorescence lifetime measurements allowed the estimate of $\tau_f$ = (1.0 ± 0.2) ns for the molecular form of asulam (**1**) in aqueous solution (see Table SI1 of the Supporting Information). Taking into account the fluorescence quantum yield and the fluorescence lifetime, the natural fluorescence lifetime ($\tau_f^0$) could be obtained as

$$\tau_f^0 = \frac{\tau_f}{\Phi_f} = \frac{1}{k_f}$$

In aqueous solution, $\tau_f^0$ is 6.5 ns; thus, a monoexponential fluorescence decay rate constant ($k_f$) of $1.5 \times 10^8$ $s^{-1}$ is obtained, not far from the value $6 \times 10^8$ $s^{-1}$ calculated from the observed absorption and fluorescence bands using the Strickler–Berg approach:[45]

$$k_f = \frac{1}{\tau_f^0} = 2.88 \times 10^{-9} n^2 \frac{\int F(\bar{\nu})\mathrm{d}\bar{\nu}}{\int \frac{F(\bar{\nu})}{\bar{\nu}^3}\mathrm{d}\bar{\nu}} \int \frac{\varepsilon(\bar{\nu})}{\bar{\nu}}\mathrm{d}\bar{\nu}$$

where $n$, $\bar{\nu}$, and $\varepsilon(\bar{\nu})$ have been previously defined (vide supra), and $F(\bar{\nu})$ is the fluorescence intensity.

The intrinsic radiative decay rate constant for fluorescence is also related to the fluorescence dipole transition moment:[33]

$$\mu_{e\to g} = \sqrt{\frac{3h\Phi_f}{64\pi^4 n^3 \tau_f \nu_{f,max}^3}}$$

A value of 2.1 D is found in aqueous solution, far from the 5.2 D obtained for the ground to excited state transition dipole moment (vide supra), suggesting electronic and geometrical relaxation from the Franck–Condon state to the lowest emitting excited state.

Although there is no phosphorescence ($P$) at room temperature, it could be observed in EtOH at 77 K (see Figure 3). The normal phosphorescence quantum yield ($\phi_P$) is given by:

$$\Phi_P = \frac{n_{ph,P}}{n_{ph,abs}} = \Phi_{ISC}\Phi'_P = \Phi_{ISC}\frac{\tau_P}{\tau_P^0}$$

where $n_{ph,P}$ is the total number of emitted phosphorescence photons, and $n_{ph,abs}$ is the total number of absorbed excitation light photons, $\Phi_{ISC}$ stands for the quantum yield of singlet–triplet intersystem-crossing, $\Phi'_P$ is the intrinsic, triplet based, phosphorescence quantum yield, and $\tau_P$ and $\tau_P^0$ are the phosphorescence and intrinsic phosphorescence lifetimes, respectively.

The obtained values for the phosphorescence lifetime and quantum yield of the molecular form of asulam (**1**) are, respectively, $\tau_P$ = (1.1 ± 0.1) s and $\phi_P$ = 0.36 (using benzophenone as reference, with $\phi_P$ = 0.84[21]). Similar phosphorescence lifetimes have been obtained for sulfanilamide and derivatives.[40]

Photophysics results imply that 16% of asulam molecules (**1**) deactivate by fluorescence, 36% through phosphorescence, and the remaining 48% uses nonradiative decay pathways, either from the singlet and the triplet states (see Theoretical Description).

A quenching effect of $O_2$ is observed on the fluorescence, more remarkable in 1-propanol and smaller in water (Table SI2 and Figure SI3 of Supporting Information). Since molecular oxygen is present as $^3O_2$ and the fluorescence is originated from the first singlet state, and taking into account the short fluorescence lifetime (1.6 ns), this deactivation effect cannot be explained as a collisional process or by long-distance interaction processes. A feasible explanation, accepted in related systems[46] is that the oxygen forms a contact charge transfer complex with asulam, which fits in well with the theoretical calculations and the solvent polarity studies.

*Solvent Effects. Solvatochromic Measurements and Dipole Moments.* The purpose of the study of steady-state Stokes shifts is to distinguish between solvent-induced and spectral shifts due to intramolecular relaxation. Interactions between solute and solvent are responsible for the Stokes shifts, i.e., the observed solvatochromism. This approach relies on the possibility of describing each solvent by one or several parameters reflecting the solvent effect on the spectra.

The excited state dipole moment can be calculated from the solvatochromic shifts of the absorption and fluorescence spectra by the solvatochromic method,[15,47−50] which involves inexpensive equipment and reflects the effect of electric field on the displacement of the absorption and emission bands. Solvatochromic shifts in absorption only give information on the variation of solvation energy occurring immediately after the molecular excitation, thus not reflecting time averaged effects that would eventually result from subsequent events. The red shift of the absorbing and emitting bands with increasing solvent polarity points to $\mu_e > \mu_g$.

Solvatochromic data are usually analyzed by variants of the method first proposed by Lippert and Mataga,[51−54] who evaluated the change in dipole moment ($\Delta\mu = \mu_e - \mu_g$) on going from the ground state (g) to the excited state (e) through a plot of the Stokes shift as a function of a macroscopic solvent polarity parameters ($n$, refractive index, and $\varepsilon$, the static electric relative permittivity, of the solvent) and by obtaining $\mu_g$ from another source, either theoretical or experimental. Here, the following equations have been used:

$$\text{Ooshika–Lippert–Mataga: } \bar{\nu}_{a,max} - \bar{\nu}_{f,max} = m_1 f_0(\varepsilon, n) + (\bar{\nu}_{a,0} - \bar{\nu}_{f,0})$$

$$\text{Bakhshiev: } \bar{\nu}_{a,max} - \bar{\nu}_{f,max} = m_2 f(\varepsilon, n) + (\bar{\nu}_{a,0} - \bar{\nu}_{f,0})$$

$$\text{Kawski–Chama–Viallet: } \bar{\nu}_{a,max} + \bar{\nu}_{f,max} = -m_3\Phi(\varepsilon, n) + (\bar{\nu}_{a,0} + \bar{\nu}_{f,0})$$


dx.doi.org/10.1021/jp311932z | J. Phys. Chem. A 2013, 117, 2125−2137

**Table 3. Parameters of the Least Squares Fittings of Mono- and Multiparameter Linear Solvation Energy Relationships to Solvatochromic Data**

| | | | | | | |
|---|---|---|---|---|---|---|
| Ooshika–Lippert–Mataga | | $\bar{\nu}_{a,max} - \bar{\nu}_{f,max} = (\bar{\nu}_{a,0} - \bar{\nu}_{f,0}) + m_1 f_0(\varepsilon, n)$ | | | $r$ | |
| | $(\nu_{0,a} - \nu_{0,f})$ (cm$^{-1}$) | $m_1$ (cm$^{-1}$) | | | 0.71 | |
| | 5824 ± 616 | 6182 ± 2345 | | | ($n$ = 9) | |
| Bakhshiev | | $\bar{\nu}_{a,max} - \bar{\nu}_{f,max} = (\bar{\nu}_{a,0} - \bar{\nu}_{f,0}) + m_2 f(\varepsilon, n)$ | | | | |
| | $(\nu_{0,a} - \nu_{0,f})$ (cm$^{-1}$) | $m_2$ (cm$^{-1}$) | | | 0.66 | |
| | 6167 ± 548 | 1744 ± 742 | | | ($n$ = 9) | |
| Kawski–Chama–Viallet | | $\bar{\nu}_{a,max} + \bar{\nu}_{f,max} = (\bar{\nu}_{a,0} + \bar{\nu}_{f,0}) - m_3 \Phi(\varepsilon, n)$ | | | | |
| | $(\nu_{0,a} + \nu_{0,f})$ (cm$^{-1}$) | $m_3$ (cm$^{-1}$) | | | −0.74 | |
| | 70945 ± 1194 | 2778 ± 965 | | | ($n$ = 9) | |
| Reichardt | | $\bar{\nu}_{a,max} - \bar{\nu}_{f,max} = (\bar{\nu}_{a,0} - \bar{\nu}_{f,0}) + m_4 E_T^N$ | | | | |
| | $(\nu_{0,a} - \nu_{0,f})$ (cm$^{-1}$) | $m_4$ (cm$^{-1}$) | | | 0.62 | |
| | 6837 ± 286 | 1106 ± 490 | | | ($n$ = 10) | |
| Kamlet–Taft | | $\bar{\nu}_{max} = \bar{\nu}_0 + a{\cdot}\alpha + b{\cdot}\beta + p{\cdot}\pi^*$ | | | | prob > F |
| absorption | $\nu_{0,a}$ (cm$^{-1}$) | $a_A$ | $b_A$ | $p_A$ | 0.28[a] | 0.55 |
| | 38463 ± 718 | 455 ± 570 | −838 ± 924 | −1234 ± 881 | ($n$ = 10) | |
| absorption[b] | 37899 ± 323 | | | −613 ± 461 | −0.43 | |
| | | | | | ($n$ = 10) | |
| emission | $\nu_{0,f}$ (cm$^{-1}$) | $a_E$ | $b_E$ | $p_E$ | 0.89[a] | 0.003 |
| | 31641 ± 431 | −73 ± 342 | −1673 ± 1094 | −1094 ± 529 | ($n$ = 10) | |
| emission[c] | 31712 ± 255 | −1776 ± 261 | −1186 ± 285 | | 0.88[a] | 0.0005 |
| | | | | | ($n$ = 10) | |
| Catalan et al. | | $\bar{\nu}_{max} = \bar{\nu}_0 + csa{\cdot}SA + csb{\cdot}SB + csp{\cdot}SP + cdsp{\cdot}SdP$ | | | | |
| absorption | $\nu_{0,A}$ (cm$^{-1}$) | $csa_A$ | $csb_A$ | $csp_A$ | $csdp_A$ | 0.21[a] | 0.85 |
| | 38970 ± 1934 | −228 ± 489 | −244 ± 627 | −1560 ± 2313 | −314 ± 793 | ($n$ = 10) | |
| emission | $\nu_{0,f}$ (cm$^{-1}$) | $csa_E$ | $csb_E$ | $csp_E$ | $csdp_E$ | 0.85[a] | 0.03 |
| | 29510 ± 1259 | −1006 ± 318 | −544 ± 408 | 1834 ± 1506 | −190 ± 516 | ($n$ = 10) | |
| emission[d] | 29299 ± 1037 | −1084 ± 221 | −500 ± 361 | 1947 ± 1364 | | 0.85[a] | 0.007 |
| | | | | | | ($n$ = 10) | |

[a]R-squared (coefficient of determination). The following independent variables are included in the statistical analysis. [b]$\pi^*$. [c]$\alpha$ and $\pi^*$. [d]SA, SB, and SP.

A brief description of these equations is presented in the Supporting Information. Static electric relative permittivity and the refractive index of the solvents used in this study are collected in Table SI3 of the Supporting Information.

Figures SI4–SI6 of the Supporting Information show the graphs of Stokes shift versus bulk solvent polarity function according to Ooshika–Lippert–Mataga, Bakhshiev, and Kawski–Chama–Viallet equations, respectively. From those graphs, $m_1$, $m_2$, and $m_3$ are obtained (Table 3).

Linear fits were poor, even excluding data from 1,4-dioxane. Poor fits have been also described for aniline and derivatives,[36] with coumarins[55] and 1,4-dioxane, behaving as an outlier.[36] The deviation observed for dioxane is consistent with the fact that it acts as a pseudopolar solvent of variable polarity function, which depends upon the solute's electric field, as a result of conformation polarizability.[56]

Likewise for aniline, solvent effects on the spectra allows considering specific solvent effects of water on asulam. The observed red-shift in its absorption band in polar solvents is ascribable to an increase in dipole moment upon excitation. The angle between the dipole moments of the emitting state and the ground state is 25°, the former being higher than the latter by 2.3 D, i.e., $\mu_e$ = 7.8 D, which is consistent with the observed red shift of the absorption and emitting bands with the polarity of the solvent. The dipole moment of the ground state was calculated theoretically, 5.51 D, using the CASPT2-(6,6)//CASSCF method and a one-electron basis set of the ANO-S type contracted to S[4s3p1d]/C,N,O[3s2p1d]/H[2s]. Table 4 shows the obtained values of $\mu_e$ and $\mu_g$, assuming, as usual, collinearity between those dipole moments and similar ground state and excited state polarizabilities, and $\Delta\mu$ using Ooshika–Lippert–Mataga equation, again $\mu_e > \mu_g$.

**Table 4. Dipole Moments of the Ground ($\mu_g$) and Excited States ($\mu_e$), Calculated Theoretically and Using the Solvatochromic Method (Assuming They Are Collinear)**

| | $a$[a] (Å) | $\mu_g$[b] (D) | $\mu_e$[b,c] (D) | $\mu_g$[d] (D) | $\mu_e$[d] (D) | $\mu_e/\mu_g$[d] | $\Delta\mu$[d] (D) | $\Delta\mu$[e] (D) | $\Delta\mu$[f] (D) |
|---|---|---|---|---|---|---|---|---|---|
| value | 4.83 | 5.5 | 8.7 | 1.3 | 5.7 | 4.4 | 4.4 | 8.3 | 1.9 |

[a]Theoretical calculation B3LYP/6-31G(+). [b]Theoretical calculation CASPT2. [c]$S_2$ level at the FC geometry, theoretical calculation CASPT2. [d]Using Bakhshiev and Kawski–Chama–Viallet equations. [e]From Lippert–Mataga equation. [f]Using Reichardt equation.

Solvent effects on the absorption and emitting bands of the molecular form of asulam (**1**) do not follow the classical behavior with bulk polarity functions, which suggests that specific solute–solvent interactions are not negligible. The oxygen atoms in sulfonyl and carbonyl groups and the lone pair electron on the nitrogens can act as hydrogen bond acceptors; moreover, the hydrogen atoms linked to the nitrogen can act as hydrogen bond donors. Thus, water and alcohols show


dx.doi.org/10.1021/jp311932z | J. Phys. Chem. A 2013, 117, 2125–2137

amphipathy in the hydrogen-bonding system (Figure 5), whereas polar aprotic solvents can form hydrogen bonds with hydrogen bond donor sites in asulam but cannot interact with hydrogen bond acceptor sites.

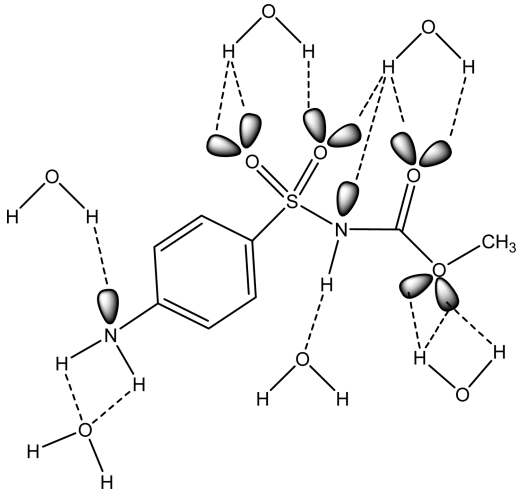

**Figure 5.** Simplified view of the different possibilities for hydrogen bonding in the ground and excited states of asulam (**1**) in aqueous solution.

A multitude of empirical single- and multiparameter solvent scales designed on the basis of solvent-dependent phenomena (spectroscopic, kinetic, and equilibrium) have been proposed to quantify solvation interactions at the molecular level.[49] These scales could be based on one single parameter, like the so-called Dimroth–Reichardt,[49] or involving multiparametric correlation equations, either by the combination of two or more existing scales or by postulating specific parameters, to unravel the effect of the medium, e.g., Kamlet et al. ($\alpha$, $\beta$, and $\pi^*$ parameters)[11−14] or Catalán et al. (*SP*, *SdP*, *SB*, and *SA*).[15]

Sometimes solvatochromic shifts of dipolar molecules correlate better with microscopic solvent polarity parameters, such as the dimensionless microscopic solvent polarity parameter $E_T^N$ proposed by Reichardt,[49] rather than with traditionally used bulk solvent polarity functions (vide supra):

$$\bar{\nu}_{a,max} - \bar{\nu}_{f,max} = m_4 E_T^N + (\bar{\nu}_{a,0} - \bar{\nu}_{f,0})$$

$E_T^N$ includes specific interactions in addition to the nonspecific solvent effects. Its value for the solvents used here are collected in Table SI3 of the Supporting Information.

A linear dependence of Stokes shifts versus $E_T^N$ was obtained for the ten solvents used in this study (see Supporting Information, Figure SI7), which is a clear evidence of the existence of specific solute–solvent interactions. From the slope $m_4$ (Table 3), the difference between dipole moments ($\mu_e - \mu_g$) is 1.9 D (Table 4), which is consistent with that obtained using bulk solvent polarity functions.

The empirical Kamlet–Abboud–Taft ($\alpha$, $\beta$, and $\pi^*$)[11−14] and Catalán et al. (*SP*, *SdP*, *SA*, and *SB*)[15] multiparameter correlations have been used to describe solute–solvent interactions at the ground and excited states. Those correlations take the form: Kamlet–Abboud–Taft

$$\bar{\nu}_{max} = \bar{\nu}_0 + a{\cdot}\alpha + b{\cdot}\beta + p{\cdot}\pi^*$$

and Catalán et al.

$$\bar{\nu}_{max} = \bar{\nu}_0 + csp{\cdot}SP + cdsp{\cdot}SdP + csa{\cdot}SA + csb{\cdot}SB$$

where $\bar{\nu}_{max}$ applies to absorption and emission.

In the Kamlet–Abboud–Taft equation, $\alpha$ and $\beta$ indicate the solvent hydrogen bond donating and accepting properties, respectively, and $\pi^*$ is a measure of the nonspecific solvent polarity/polarizability, whereas *a*, *b*, and *p* are coefficients related to solute properties: *a* measures the tendency of the solute to accept a hydrogen bond from the solvent, *b* evaluates its ability to donate a hydrogen bond to the solvent, and *p* refers to the solute dipole moment.

Similarly, Catalán et al. proposed a generalized treatment of the solvent effect based on a set of four empirical, independent solvent scales: *SdP*, *SP*, *SA*, and *SB* characterize the dipolarity, polarizability, acidity, and basicity, respectively, of a certain solvent. Kamlet–Abboud–Taft solvatochromic parameters $\alpha$, $\beta$, and $\pi^*$ are taken from ref 57, and the Catalán's *SA* and *SB* parameters were collected from refs 58–60, the solvent polarizability parameters *SP* from ref 61, and the recently proposed *SdP* solvent parameters from ref 62; all are compiled in Table SI3 of the Supporting Information.

The statistical results of the Kamlet–Abboud–Taft and Catalán et al. multiparameter correlations are presented in Table 3. Kamlet–Abboud–Taft and Catalán et al. equations exhibit very poor correlations for absorption. Although no quantitative conclusions can be drawn from them, the negative value of $p_A$ regression coefficient implies a red-shift in $\bar{\nu}_{max,a}$ as the solvent polarity/polarizability ($\pi^*$) increases. However, coefficients $a_A$ (<0) and $b_A$ (>0) imply a blue shift in $\bar{\nu}_{max,A}$ for solvents with higher hydrogen bond donating capacity, and a red-shift in $\bar{\nu}_{max,a}$ as the hydrogen bond acceptor ability of the solvent increases. The higher absolute value of $p_A$ than those of $a_A$ and $b_A$ indicates that solvent polarity/polarizability shows more effect on $\bar{\nu}_{max,a}$ than its acid–base properties. A similar conclusion can be drawn from the Catalán et al. multiparameter correlation for absorption (Table 3).

Better correlations are obtained for emission. In the case of Kamlet–Abboud–Taft equation, the main effect, bathochromic, is attributed to the ability of asulam to act as hydrogen bond donor to the solvent. The quantitative estimation of the parameters of the Catalán et al. equation points to the hydrogen-bond donor ability of the solvent as the primary factor governing the solvatochromic effect of the excited state. This is reflected by the statistical significance and magnitude of the parameter $a_A$ (Table 3) and is consistent with the increase of p$K_a$ in the excited state (vide supra). Contrary to absorption, an increase in the polarizability of the solvent destabilizes the excited state, whereas such change in its dipolarity has no effect, i.e., it does not depend on the dipole moment change of the molecular structures involved in the electronic transition.

Notice that uncertainties in solvatochromic data of **1** can come from the unaccounted content of both the protonated (**3**) and anionic (**2**) forms of asulam in protic solvents (e.g., p$K_a$ (**3**) = 1.4 and p$K_a$ (**1**) = 4.1 in water),[28] which could lead to low correlation coefficients. Kamlet–Abboud–Taft and Catalán et al. results show the same trends, and although no good statistical correlations are obtained, both approaches allow drawing interesting conclusions, and they are a bit more reliable than those involving bulk solvent polarity functions or the microscopic solvent polarity parameter $E_T^N$

**B. Theoretical Description.** *Geometric Changes.* Upon excitation, some geometrical changes take place on the amino group. A decrease in the planarity of the amino group is


dx.doi.org/10.1021/jp311932z | J. Phys. Chem. A 2013, 117, 2125−2137

obtained on going from the ground state to the equilibrated excited states (Table 5), which implies less delocalization of the lone pair of the amino nitrogen onto the aromatic $\pi$ system.

**Table 5. Relevant Theoretical Geometrical Parameters of the Amino Group of the Molecular Form of Asulam (1) (See the Text and Figure 6)**

| parameter | $S_0/S_2$ ($^1L_a$) | $S_1$ ($^1L_b$) | $T_1$ ($^3L_a$) | $T_2$ ($^3L_b$) |
|---|---|---|---|---|
| $A_1$ (deg) | 116.6 | 112.8 | 112.4 | 113.5 |
| $A_2$ (deg) | 116.6 | 112.9 | 112.5 | 113.5 |
| $A_3$ (deg) | 113.0 | 109.7 | 109.1 | 110.5 |
| ($A_1 + A_2 + A_3$) (deg) | 346.2 | 335.3 | 333. 9 | 337.5 |
| % planarity | 96.2 | 93.1 | 92.7 | 93.8 |
| $w_1$ (deg) | −22.1 | −29.6 | −45.6 | −27.7 |
| $w_2$ (deg) | 22. 5 | 30.4 | 42.7 | 29.0 |
| $\tau$ (deg) | 0.2 | 0.4 | −1.4 | 0.7 |
| $w_3$ (deg) | 177.6 | 176.0 | 155.7 | 176.3 |
| $d_{C7-N10}$ (Å) | 1.385 | 1.397 | 1.402 | 1.390 |

As shown in Figure 6, the planarity of the amino group is defined in percent as $\{(A_1 + A_2 + A_3)/360°\} \times 100$, $A_i$ being

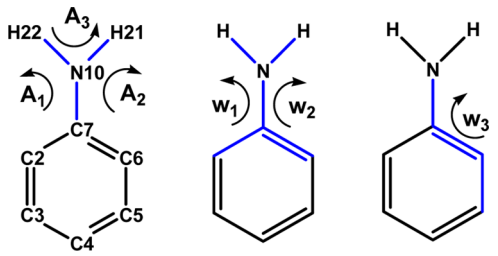


**Figure 6.** Blue lines indicate the atoms defining the angles involved in the determination of the planarity/pyramidalization of the amino group, its twist angle ($\tau$), and the coplanarity ($w_3$) of the amino group and the phenyl ring around carbon−nitrogen (C7−N10) bond.

the angles (deg) C7−N10−H22 ($A_1$), C7−N10−H21 ($A_2$), and H22−N10−H21 ($A_3$). The decrease in the Mulliken's negative charge (see Supporting Information, Table SI4) on the amino nitrogen in going from the ground state (−0.7760) to excited states (FC = −0.7144; S1 = −0.7383) is in agreement with the increased amino group pyramidalization upon excitation.

The twist angle of the amino group is close to zero for all states, and the bond length between the phenyl ring and the amino group (C7−N10) follows the expected trend with excitation (Table 5). The twist angle of the amino group ($0° < \tau = (w_1 + w_2)/2 < 90°$) is calculated according to Ferreti et al.,[63] where the dihedrals angles (deg) $w_1$ and $w_2$ are C2−C7−N10−H22 and C6−C7−N10−H21, respectively (Figure 6).

The amino group is almost coplanar to the phenyl ring, but the lowest triplet state where the nitrogen lies well above the plane is defined by the carbons of the phenyl group (Table 5), which is also consistent with its increased pyramidalization; the dihedral angle (deg) $w_3$ (C5−C6−C7−N10) is used as a simple index of the planarity of the system formed by the phenyl ring and the nitrogen of the amino group (Figure 6).

*Photophysics.* The photophysics of asulam starts with absorption of near-UV radiation at the Franck−Condon (FC) ground-state geometry of the molecule. Two low-lying singlet excited states, labeled as $S_1$ ($^1L_b$ $\pi\pi^*$) and $S_2$ ($^1L_a$ $\pi\pi^*$) using Platt's nomenclature,[64] have been computed at the CASPT2 level at 4.36 (284 nm) and 5.02 eV (247 nm), respectively. The labeling derives from the composition of the CASSCF wave function as displayed in Table 6.

The transition to the $S_1$ ($^1L_b$ $\pi\pi^*$) state, mainly described as the antisymmetric combination of the HOMO (H) → LUMO (L) + 1 (34%) and H − 1 → L (27%) one-electron promotions, has a corresponding oscillator strength lower than $10^{-3}$. On the contrary, the $S_2$ ($^1L_a$ $\pi\pi^*$) state, with a CASSCF wave function basically composed by the H → L (56%) configuration, has a related oscillator strength of 0.15, and consequently, it will be the bright state initially populated in this range of energies and from which the photochemical events will take place; this is also supported by the lack of mirror symmetry between the absorption and emission spectra (Figure 3).

The absorption band maximum observed in chloroform at 4.68 eV (265 nm) is therefore clearly assigned to the $S_2$ ($^1L_a$ $\pi\pi^*$) state. The vertical excitation energy, 5.02 eV (247 nm), computed *in vacuo* is, as usual, placed slightly higher than the band maximum. A third singlet excited state $S_3$ ($^1B_b$ $\pi\pi^*$), formed by the symmetric combination of the H → L + 1 and H − 1 → L configurations, is computed much higher in energy, 6.51 eV (190 nm) with also a large related oscillator strength of 0.17. Regarding the triplet states, and as it is typical is $\pi$-conjugated organic molecules, a low-lying vertical excitation is computed for the $T_1$ ($^3L_a$ $\pi\pi^*$) at 3.64 eV, well below the other states. Two other triplet states follow in energy, $T_2$ ($^3L_b$ $\pi\pi^*$) and $T_3$ ($^3B_a$ $\pi\pi^*$), at 4.19 (296 nm) and 4.27 eV (290 nm), respectively. A fourth triplet states is computed higher than the two lowest singlet states, at 5.01 eV (247 nm). The energy gap between the initially populated $S_2$ state (in the low-energy

**Table 6. Calculated Vertical Excitation Energies at the FC Geometry ($E_{VA}$) for the Lowest Valence Singlet and Spin Forbidden Triplet States; the Related Experimental Values Are Also Included**

| | theoretical | | | | exptl |
|---|---|---|---|---|---|
| state | $E_{VA}$ (eV(nm)) | $f$ | $\mu$ (D) | main configurations | $A_{max}$ (eV(nm)) |
| $S_0$ | | | 5.51 | | |
| $T_1$ ($^3L_a$ $\pi\pi^*$) | 3.64 (340) | | 5.20 | H → L(53%); H − 1 → L + 1(22%) | |
| $T_2$ ($^3L_b$ $\pi\pi^*$) | 4.19 (296) | | 5.45 | H → L + 1(47%); H − 1 → L(31%) | |
| $T_3$ ($^3B_a$ $\pi\pi^*$) | 4.27 (290) | | 5.74 | H − 1 → L + 1(57%); H → L(22%) | |
| $S_1$ ($^1L_b$ $\pi\pi^*$) | 4.36 (284) | $<10^{-3}$ | 5.26 | H → L + 1(34%); H − 1 → L(27%) | |
| $T_4$ ($^3B_b$ $\pi\pi^*$) | 5.01 (247) | | 7.71 | H → L + 1(29%); H − 1 → L(39%) | |
| $S_2$ ($^1L_a$ $\pi\pi^*$) | 5.02 (247) | 0.15 | 8.70 | H → L (56%); H → L + 1(15%) | 4.64(265)[a] |
| $S_3$ ($^1B_b$ $\pi\pi^*$) | 6.51 (190) | 0.17 | 5.89 | H → L + 1(21%); H − 1 → L(20%) | |

[a]Absorption band maximum in chloroform. Estimated oscillator strength: 0.43.


dx.doi.org/10.1021/jp311932z | J. Phys. Chem. A 2013, 117, 2125−2137

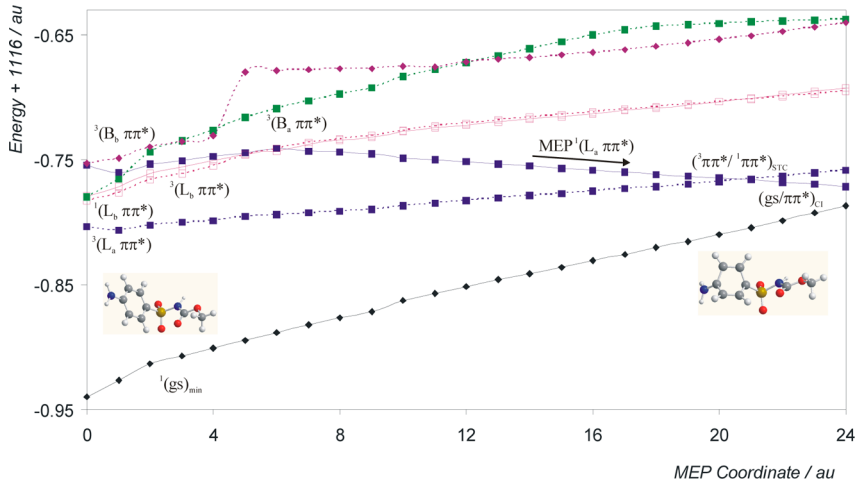


**Figure 7.** CASPT2 low-lying singlet and triplet states of asulam along the minimum energy path computed from the FC geometry on the $^1(L_a\ \pi\pi^*)$ state of asulam: singlet states, solid lines, and triplet states, dotted lines.

region of the spectrum) and the triplet states is large (>0.65 eV) except for $T_4$. As expected from the qualitative El Sayed rules,[65] all spin−orbit coupling (SOC) terms are, however, too low in the FC region (<0.30 $cm^{-1}$) to promote efficient ISC processes, which should take place instead along the deactivation path of $S_2$. Certainly, all the states found at low-energies have a $\pi\pi^*$ character, and therefore SOC interaction is small, whereas $n\pi^*$ or $\pi\sigma^*$ states have been estimated much higher in energy.

The computed dipole moments of the different excited states are similar to that of the ground state, 5.51 D. Exceptions are the $S_2$ ($^1L_a\ \pi\pi^*$) and $T_4$ ($^3B_b\ \pi\pi^*$) states, which exhibit large dipole moments of 8.70 and 7.71 D, respectively. The analysis of the correlation between the Stokes shift (computed as difference between absorption and fluorescence maxima) in terms of bulk solvent polarity functions and of the microscopic solvent polarity parameter $E_T^N$ (vide supra) yielded a difference of around 2 D (Table 4), supposedly between the ground and lowest singlet excited state dipole moments. In fact, as it will be shown later, the origin of the absorption and fluorescence bands relies on two different states, ($^1L_a\ \pi\pi^*$) and ($^1L_b\ \pi\pi^*$), respectively. Despite such large differences and the establishment undergone by the $S_2$ ($^1L_a\ \pi\pi^*$) band in the presence of polar solvents, no relevant changes can be expected in the initial population pattern, considering the large gap between $S_2$ and the other states. As a matter of fact, and except for protic solvents like water, the absorption band maxima changes less than 0.1 eV in environments of different polarity.

In order to study the photophysical events, the main reaction decay pathway of the spectroscopic $S_2$ ($^1L_a\ \pi\pi^*$) state has to be determined. Figure 7 displays the CASPT2 energies of the low-lying singlet and triplet states of asulam obtained along the CASSCF MEP on the $S_2$ ($^1L_a\ \pi\pi^*$) state computed from the FC region. Although a small energy barrier can be observed along the path of the state, this feature has a minor significance because it is probably caused by unbalances between the initial $S_0$ DFT geometry, the computed CASSCF steepest-descendent MEP, and the CASPT2 point energies.

The path can be considered essentially barrierless from the FC structure toward the region of the CI between the ground and the lowest singlet excited state, named $(gs/\pi\pi^*)_{CI}$ or $(S_0/S_1)_{CI}$ ($S_1$ now being the vertical $S_2$ state).

Figure 8 displays the geometries for asulam at the ground state minimum and at the $(gs/\pi\pi^*)_{CI}$ (see also Supporting

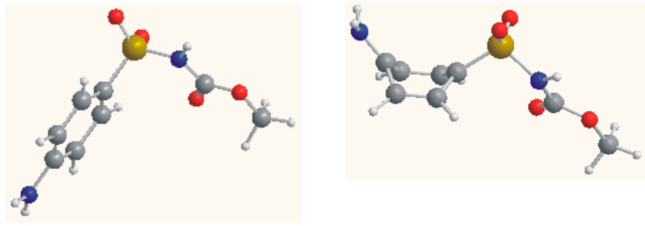

**Figure 8.** Optimized structures of asulam at the ground state minimum, $(gs)_{min}$ (left) and at the conical intersection $(gs/\pi\pi^*)_{CI}$ (right).

Information, Table SI5). The latter has been computed independently as a MECP between the $S_0$ and $S_1$ states and located at 4.12 eV (adiabatically from the ground state minimum) with a structure close to that of the molecule at the end of the MEP. The main distortion undergone by the system along the path has taken place on the benzene ring, which has adopted a boat-like $^{1,4}B$ conformation,[66] a diradicaloid-type structure known in the photochemistry of benzene to be a funnel for the radiationless decay to the ground state.[67]

The singlet state relaxation along a barrierless path leading to conical intersections with two low-lying singlet states can be expected to be very efficient and, correspondingly, the nonadiabatic decay effects in the CI region. Several singlet and triplet states are crossed; however, during the evolution of the system, an efficient population transfer can take place (see Figure 7) near the crossing regions. Close to point 5 of the MEP, a degeneracy region between the $S_2$ ($^1L_a\ \pi\pi^*$) and $S_1$ ($^1L_b\ \pi\pi^*$) states occurs. From this point, a MEP computed on the $S_1$ ($^1L_b\ \pi\pi^*$) state hypersurface (see Supporting Information, Figure SI8) leads directly to the minimum of the state, computed adiabatically at 4.39 eV ($T_e$, 282 nm) with a vertical emission of 4.07 eV (304 nm). Such values can be successfully compared with the fluorescence data obtained in chloroform, yielding band origins and maximum of 4.13 ($T_0$, 300 nm) and 3.83 eV (324 nm), respectively (see Tables 1 and 7). As the agreement is good enough and no low-lying energy minimum has been located for the $S_2$ ($^1L_a\ \pi\pi^*$) state, it can be


dx.doi.org/10.1021/jp311932z | J. Phys. Chem. A 2013, 117, 2125−2137

**Table 7. Calculated Vertical Excitation Energies at the FC Geometry ($E_{VA}$), Electronic Band Origins ($T_e$), and Vertical Emission Energies ($E_{VE}$) for the Lowest Valence Singlet and Spin Forbidden Triplet States; the Related Experimental Values Are Also Included**

| | theoretical (eV (nm)) | | | experimental (eV (nm)) | | |
|---|---|---|---|---|---|---|
| state | $E_{VA}$ | $T_e$ | $E_{VE}$ | $A_{max}$ [a] | $T_0$ [a] | $E_{max}$ [a] |
| $T_1$ ($^3L_a$ $\pi\pi^*$) | 3.64 (340) | 3.61 (343) | 2.78 (445) | | 3.44 (360) [b,c] | 2.82 (439) [b,c] |
| $T_2$ ($^3L_b$ $\pi\pi^*$) | 4.19 (296) | 4.23 (292) | 3.92 (316) | | | |
| $T_3$ ($^3B_a$ $\pi\pi^*$) | 4.27 (290) | | | | | |
| $S_1$ ($^1L_b$ $\pi\pi^*$) | 4.36 (284) | 4.39 (282) | 4.07 (304) | | 4.13 (300) [b,d] | 3.83 (324) [b,d] |
| $S_2$ ($^1L_a$ $\pi\pi^*$) | 5.01 (247) | [e] | [e] | 4.68 (264) [b] | | |
| $T_4$ ($^3B_b$ $\pi\pi^*$) | 5.02 (247) | | | | | |
| $S_3$ ($^1B_b$ $\pi\pi^*$) | 6.51 (190) | | | | | |

[a]Measured absorption band maximum ($A_{max}$), band origin ($T_0$), and fluorescence maximum ($E_{max}$). [b]In water ($T_1$) and chloroform ($S_1$ and $S_2$). [c]Computed (83.4 s) and experimental (2.58 s) phosphorescence radiative lifetimes ($\tau_{Prad}$). [d]Computed (3858 ns) and experimental (6.25 ns) fluorescence radiative lifetime ($\tau_{Frad}$). The Strickler-Berg model is not applicable here due to the high nonradiative rates. See text. [e]For the isolated molecule, the MEP on $S_2$ ($^1L_a$ $\pi\pi^*$), after crossing with all other excited states, leads directly to a conical intersection with the ground state, $(S_0/S_1)_{CI}$, placed adiabatically at 4.12 eV.

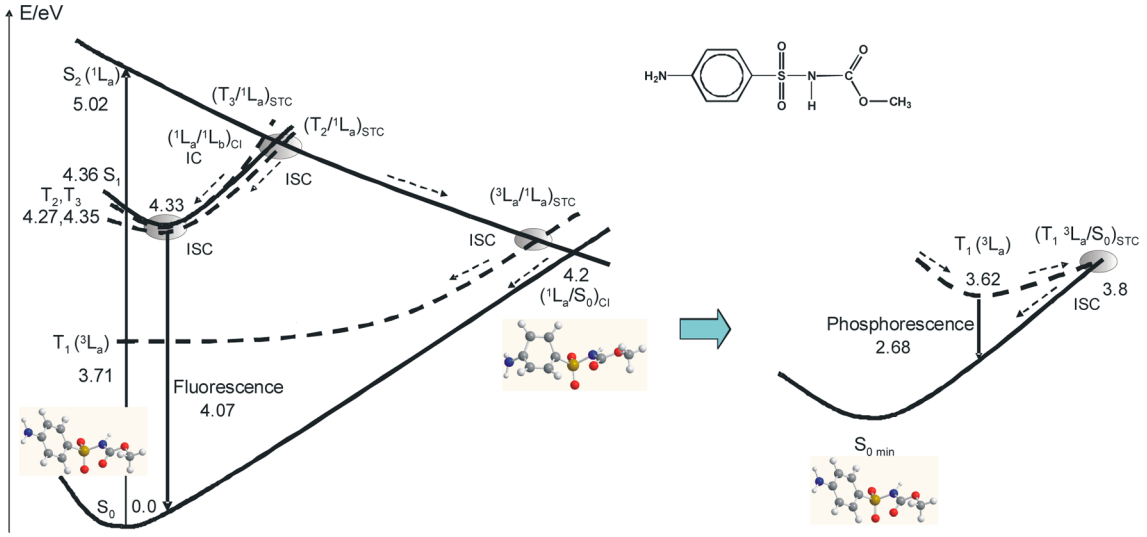


**Figure 9.** Summary of the photophysics of asulam based on the CASPT2 results.

safely assumed that the $S_1$ ($^1L_b$ $\pi\pi^*$) state is the protagonist of the fluorescence. The state minimum displays a dipole moment similar to that of the ground state (4.91 D), and therefore, the emission band should not be strongly affected by the polarity of the solvent. Indeed, the fluorescence maximum shifts by less than 0.1 eV in different environments.

Fluorescence in asulam is, however, weak. The emission quantum yield $\phi_f$ has been measured to increase with the polarity of the solvent: 0.032 in acetonitrile, 0.099 in ether, and 0.155 in water.

Considering the low sensitivity of the $S_1$ ($^1L_b$ $\pi\pi^*$) emission band on the solvent polarity, the increase on the quantum yield should be related to the stabilization of the highly polar $S_2$ ($^1L_a$ $\pi\pi^*$) state and, accordingly, of the conical intersection $(S_1/S_2)_{CI}$ triggering the population switch from $S_2$ to $S_1$ along the decay of the higher singlet state. The low fluorescence quantum yield also points to the presence of efficient nonradiative decay channels. The theoretical fluorescence radiative lifetime, computed by means of the Strickler−Berg approximation as 3858 ns (as a logical consequence of the low transition dipole moment relating $S_0$ and $S_1$), is of the same order (i.e., in the nanosecond time scale) as it is the estimated value in water, 6.25 ns. Theoretical prediction is considerably larger that the available experimental datum that has been also found previously in systems characterized by the presence of important nonradiative paths.[30,45,68] Nevertheless, as suggested by one of the reviewers, it is also worth pointing out that, since different states are involved in absorption and emission, it is difficult to deconvolute these in the extinction coefficient used in the Strickler−Berg approximation.

Along the evolution through the $S_2$ ($^1L_a$ $\pi\pi^*$) state decay, four triplet states are crossed, one at the beginning (~5.0 eV), $T_4$ ($^3B_b$ $\pi\pi^*$), then $T_3$ ($^3B_a$ $\pi\pi^*$) and $T_2$ ($^3L_b$ $\pi\pi^*$), and finally the $T_1$ ($^3L_a$ $\pi\pi^*$) state close to the end of the path (~4.5 eV), that is, near the conical intersection $(gs/\pi\pi^*)_{CI}$ and displaying, therefore, a similar structure. The computed electronic SOC terms between the $S_2$ ($^1L_a$ $\pi\pi^*$) and the different triplet states at the corresponding STC regions are somewhat low (<0.3 $cm^{-1}$), although such values are probably underestimated because the relative small number of states included in the coupling (four singlet and four triplet states, all of $\pi\pi^*$ type). In any case, the computed overall ISC rate at each of the STC regions is expected to become large enough to guarantee efficient processes once the vibrational effects and density of states are taken into account in the SOC coupling, as it has been established in a number of systems.[69] We have followed


dx.doi.org/10.1021/jp311932z | J. Phys. Chem. A 2013, 117, 2125−2137

respective MEPs from the STC crossings between $S_2$ ($^1L_a$ $\pi\pi^*$) and $T_2$ and $T_1$, which display the largest SOC values in the crossing regions (~0.3 $cm^{-1}$ in both cases). The $T_2$ state evolves toward its minimum, as shown by computing the corresponding MEPs (see Supporting Information, Figure SI9), and finally, it decays to the lowest $T_1$ triplet state through an efficient triplet−triplet IC processes because the corresponding $(T_2/T_1)_{CI}$ lies close by the $T_2$ minimum (see Supporting Information, Figure SI10). The second MEP computed leads the $T_1$ ($^3L_a$ $\pi\pi^*$) from the $(S_2/T_1)_{STC}$ toward the triplet state minimum (see Supporting Information, Figure SI11). In either case, IC from $T_2$ or ISC from $S_2$, the $T_1$ ($^3L_a$ $\pi\pi^*$) will decay to its own minimum and become phosphorescent (see Figure 9).

Considering the different energy ranges in which the STC regions are located, it can be expected for the triplet quantum yield to be wavelength dependent, an effect and a mechanism present in molecules like thymine, uracil, or adenine.[70,71] Regarding the parameters computed for the phosphorescence, the band origin, 3.61 eV ($T_e$, 343 nm), and vertical emission, 2.78 eV (445 nm), are in good correspondence with the experimental values in water, 3.44 (360 nm) and 2.82 eV (439 nm), respectively.

Part of the population of the triplet states may also decay back to the original ground state through a nonradiative process. In fact, the $T_1$ minimum might reach an intersystem crossing region between the $T_1$ and the ground state, ($^1$gs/$^3L_a$ $\pi\pi^*$)STC, surmounting a small barrier of 0.41 eV (10 kcal $mol^{-1}$) (see Supporting Information, Figure SI12). The ISC funnel in which the electronic SOC has been computed as 0.86 $cm^{-1}$ favoring then the energy transfer is easily accessible with the available excess energy and, consequently, contributes to the large ratio of radiatonless decay experimentally determined (0.48).

The presented photoprocesses that the system may undergo are resumed in Figure 9, which displays a scheme of the photophysics of asulam based on CASPT2 results. Once again the CASPT2 method reveals more appropriate to describe excited states than lower-level methods used in the past with this compound.[72,73]

Notice that the main charge transfer takes place between C4 and C7 (see Supporting Information, Table SI4); in going from the ground to the $S_2$ ($^1L_a$ $\pi\pi^*$) state at the FC, geometry C4 doubles its negative charge and then suffers a 3-fold reduction at $S_1$ ($^1L_b$ $\pi\pi^*$); however, C7 becomes twice its positive charge at $S_2$ ($^1L_a$ $\pi\pi^*$) state at the FC geometry, which reduces 6-fold at $S_1$ ($^1L_b$ $\pi\pi^*$); the charge separation, larger at the $S_2$ state at the FC region than at the minimum of $S_1$ state, is consistent with the higher dipole moment calculated for $S_2$.

Results are consistent with the significant role of the singlet−triplet intersystem crossings in the asulam's photophysics and photochemistry as follows from the experimental values measured here: a limited fluorescence quantum yield ($\phi_f$ = 0.18 at 298 K), a moderate phosphorescence quantum yield of 0.36 at 77 K, and the published 3-fold reduction in the photolytic quantum yield in going from a deoxygenated ($\phi_{photolysis}$ = 0.57) to a oxygen saturated aqueous solution ($\phi_{photolysis}$ = 0.17),[8] molecular oxygen ($^3O_2$) being a well-known triplet quencher.[30]

## CONCLUSIONS

Experimental and quantum chemistry methods, at the CASPT2 level, have been performed in order to study the photophysical behavior of asulam, mainly in its molecular form (**1**).

Absorption maximum wavelengths, ascribed to a $\pi \rightarrow \pi^*$ aromatic electronic transition, showed a weak red-shift upon increasing the polarity of the solvent, except for ethanol, whereas its fluorescence emission peak underwent a larger red-shift as solvent polarity rises. Linear regressions analyzing solvent effects on absorption and fluorescence spectra with the solvatochromic method in terms of bulk polarizability of the solvent or including solute−solvent specific interactions (multiparamenter approaches of Kamlet−Abboud−Taft and Catalán et al.) give poor results, likely due to the existence of many sites that may specifically interact with the solvent. Results from these multiparameter approaches are, however, in agreement with the observed increase in $pK_a$ on going from the ground state to the excited state, $\Delta pK_a$ (= $pK_a^* - pK_a$), ca. 3.

Red spectral shifts on increasing the solvent polarity implies the ground state is less polar than the excited singlet state ($\mu_g < \mu_e$), which is consistent with the rise of the dipole moment determined both empirically from solvatochromic data and theoretically at the CASPT2 level. Comparison of the modified absorption and the fluorescence spectra shows a lack of mirror image symmetry, which reflects different nuclear configurations in the absorbing and emitting states. The same conclusion is derived from either the experimental transition dipole moments and the theoretical calculations, two distinct electronic transitions have to be considered for absorption and emission. Two low-lying singlet excited states, labeled as $S_1$ ($^1L_b$ $\pi\pi^*$) and $S_2$ ($^1L_a$ $\pi\pi^*$), have been characterized. The absorption band maximum has been assigned to the $S_2$ ($^1L_a$ $\pi\pi^*$) state, whereas the lowest-lying state $S_1$ ($^1L_b$ $\pi\pi^*$) is responsible for the fluorescence spectrum. Fluorescence quantum yield at room temperature is low and varies with the solvent, highest in water ($\phi_f$ = 0.16) and independent of its acidity (3 < pH < 11), and lowest in methanol and 1-propanol ($\phi_f$, ca. 0.02). Fluorescence lifetime in aqueous solution is 1 ns ($k_f = 1.5 \times 10^{-8}$ $s^{-1}$). There is an efficient intersystem crossing from the phosphorescence quantum yield found in glassy ETOH ($\phi_P$ = 0.36) at 77 K, the phosphorescence lifetime being 1.1 s. Thus, the remaining 48% decays through nonradiative pathways. In agreement with such outcomes, the decay pathway of the spectroscopic $S_2$ ($^1L_a$ $\pi\pi^*$) state can be considered barrierless from the FC structure toward the region of the internal conversion between the ground and the lowest singlet excited state, $(gs/\pi\pi^*)_{CI}$. Along the main decay path, the presence of a conical intersection between the two low-lying singlet excited states switched part of the population to the fluorescent ($^1L_b$ $\pi\pi^*$) state, which decays to its emitting minimum. Different intersystem crossing regions have been also characterized on the potential energy hypersurface connecting the FC region and the $(gs/\pi\pi^*)_{CI}$, which account for the phosphorescent features experimentally detected. Finally, the minimum of the emitting triplet state might reach an intersystem crossing region $(^1gs/^3L_a$ $\pi\pi^*)_{STC}$ surmounting a barrier of 0.41 eV, which constitutes a second nonradiative decay path to the ground state.

Molecular-level understanding of the underlying photophysics provides clues to unveil the photodegradation pathways and certainly represents an added value in the design of new biocides.

## ASSOCIATED CONTENT

### Supporting Information

Abbreviations, additional computational details, Figures SI1 to SI13 and Tables SI1 to SI5. This material is available free of charge via the Internet at http://pubs.acs.org.


dx.doi.org/10.1021/jp311932z | J. Phys. Chem. A 2013, 117, 2125−2137

## AUTHOR INFORMATION


### Corresponding Author

*E-mail: arturo.santaballa@udc.es (J.A.S.); angelo.giussani@uv.es (A.G.).


### Notes

The authors declare no competing financial interest.

Dr. Luís Serrano-Andrés passed away on September 17th, 2010.

## ACKNOWLEDGMENTS


Financial support is acknowledged from projects CTQ2010-14892, CTQ2007-61260, and CSD2007-0010 of the Consolider-Ingenio in Molecular Nanoscience of the Spanish MEC/FEDER and PGIDIT05TAM10301PR of the Xunta de Galicia (Spain). Thanks are given to the Centro de Supercomputación de Galicia (CESGA) for computing facilities. A.F.-C. acknowledges the research grant (Formación Personal Investigador) of the former Spanish Ministerio de Educación y Ciencia. Finally, we wish to thank Professor Dr. Manuela Merchán (University of Valencia, Spain) for proof reading the manuscript and the reviewers for their helpful comments.


## REFERENCES


(1) Jha, M. N.; Mishra, S. K. Decrease in Microbial Biomass Due to Pesticide Application/Residues in Soil Under Different Cropping Systems. *Bull. Environ. Contam. Toxicol.* **2005**, *75*, 316−323.

(2) Gevao, B.; Semple, K. T.; Jones, K. C. Bound Pesticide Residues in Soils: a Review. *Environ. Pollut.* **2000**, *108*, 3−14.

(3) Official Journal of the European Union. http://eur-lex.europa.eu/LexUriServ/LexUriServ.do?uri=OJ:L2011:275:0023:0024:EN:PDF (accessed 13 Feb 2013).

(4) European Food Safety Authority. Conclusion on the Peer Review of the Pesticide Risk Assessment of the Active Substance Asulam. *EFSA J.* **2010**, *8*, 1822.

(5) Tomašević, A. V.; Gašić, S. M. Photoremediation of Carbamate Residues in Water. In *Insecticides: Basic and Other Applications*; Larramendy, S. S. M., Ed.; InTech: Rijeka, Croatia, 2012; pp 39−60.

(6) Catastini, C.; Sarakha, M.; Mailhot, G.; Bolte, M. Iron (III) Aquacomplexes as Effective Photocatalysts for the Degradation of Pesticides in Homogeneous Aqueous Solutions. *Sci. Total Environ.* **2002**, *298*, 219−228.

(7) Franck, R.; Klopffer, W. Spectral Solar Photon Irradiance in Central Europe and the Adjacent North Sea. *Chemosphere* **1988**, *17*, 985−994.

(8) Catastini, C.; Sarakha, M.; Mailhot, G. Asulam in Aqueous Solutions: Fate and Removal Under Solar Irradiation. *Int. J. Environ. Anal. Chem.* **2002**, *82*, 591−600.

(9) US Environmental Protection Agency. www.epa.gov/oppsrrd1/REDs/0265.pdf (accessed 13 Feb 2013).

(10) Kawski, A.; Bojarski, P. Comments on the Determination of Excited State Dipole Moment of Molecules using the Method of Solvatochromism. *Spectrochim. Acta, Part A* **2011**, *82*, 527−528.

(11) Kamlet, M. J.; Abboud, J. L.; Abraham, M. H.; Taft, R. W. Linear Solvation Energy Relationships. 23. A Comprehensive Collection of the Solvatochromic Parameters, $\pi^*$, $\alpha$, and $\beta$, and Some Methods for Simplifying the Generalized Solvatochromic Equation. *J. Org. Chem.* **1983**, *48*, 2877−2887.

(12) Kamlet, M. J.; Abboud, J. L.; Taft, R. W. The Solvatochromic Comparison Method. 6. The $\pi^*$ Scale of Solvent Polarities. *J. Am. Chem. Soc.* **1977**, *99*, 6027−6038.

(13) Kamlet, M. J.; Dickinson, C.; Taft, R. W. Linear Solvation Energy Relationships Solvent effects on Some Fluorescence Probes. *Chem. Phys. Lett.* **1981**, *77*, 69−72.

(14) Marcus, Y.; Kamlet, M. J.; Taft, R. W. Linear Solvation Energy Relationships: Standard Molar Gibbs Free Energies and Enthalpies of Transfer of Ions from Water into Nonaqueous Solvents. *J. Phys. Chem.* **1988**, *92*, 3613−3622.

(15) Catalán, J.; de Paz, J. L. G.; Reichardt, C. On the Molecular Structure and UV/vis Spectroscopic Properties of the Solvatochromic and Thermochromic Pyridinium-*N*-phenolate Betaine Dye B30. *J. Phys. Chem. A* **2010**, *114*, 6226−6234.

(16) Merchán, M.; Serrano-Andrés, L. Ab Initio Methods for Excited States. In *Computational Photochemistry*; Olivucci, M, Ed.; Elsevier: Amsterdam, The Netherlands, 2005; Vol. *16*, pp 35−91.

(17) Serrano-Andrés, L.; Merchán, M. Photostability and Photoreactivity in Biomolecules: Quantum Chemistry of Nucleic Acid Base Monomers and Dimers. In *Radiation Induced Molecular Phenomena in Nucleic Acids*; Leszczynski, J, Shukla, M., Eds.; Springer: Amsterdam, The Netherlands, 2008; pp 435−472.

(18) Giussani, A.; Merchán, M.; Roca-Sanjuán, D.; Lindh, R. Essential on the Photophysics and Photochemistry of the lndole Chromophore by Using a Totally Unconstrained Theoretical Approach. *J. Chem. Theory Comput.* **2011**, *7*, 4088−4096.

(19) Migani, A.; Bearpark, M. J.; Olivucci, M.; Robb, M. A. Photostability versus Photodegradation in the Excited-State Intramolecular Proton Transfer of Nitro Enamines: Competing Reaction Paths and Conical Intersections. *J. Am. Chem. Soc.* **2007**, *129*, 3703−3713.

(20) Williams, A. T. R.; Winfield, S. A.; Millar, J. N. Relative Fluorescence Quantum Yields Using a Computer-Controlled Luminescence Spectrometer. *Analyst* **1983**, *108*, 1067−1071.

(21) Murov, S. L.; Carmichael, I.; Hug, G. L. *Handbook of Photochemistry*; Marcel Dekker, Inc.: New York, 1993.

(22) Roos, B. O.; Fülscher, M. P.; Malmqvist, P-Å.; Serrano-Andrés, L.; Pierloot, K.; Merchán, M. Multiconfigurational Perturbation Theory: Applications in Electronic Spectroscopy. *Adv. Chem. Phys.* **1996**, *93*, 219−331.

(23) Serrano-Andrés, L.; Merchán, M.; Nebot-Gil, I.; Lindh, R.; Roos, B. O. Towards an Accurate Molecular-Orbital Theory for Excited-States: Ethene, Butadiene, and Hexatriene. *J. Chem. Phys.* **1993**, *98*, 3151−3162.

(24) Serrano-Andrés, L.; Merchán, M.; Borin, A. C. Adenine and 2-Aminopurine: Paradigms of Modern Theoretical Photochemistry. *Proc. Natl. Acad. Sci. U.S.A.* **2006**, *103*, 8691−8696.

(25) Serrano-Andrés, L.; Merchán, M.; Lindh, R. Computation of Conical Intersections by using Perturbation Techniques. *J. Chem. Phys.* **2005**, *122*, 104−107.

(26) Aquilante, F.; De Vico, L.; Ferré, N. MOLCAS 7. The Next Generation. *J. Comput. Chem.* **2010**, *31*, 224−247.

(27) Frisch, M. J.; Trucks, G. W.; Schlegel, H. B.; et al. *Gaussian 09*; Gaussian Inc.: Wallingford, CT, 2009 (complete reference can be found in Supporting Information ref 14).

(28) Vulliet, E.; Emmelin, C.; Chovelon, J.-M. Influence of pH and Irradiation Wavelength on the Photochemical Degradation of Sulfonylureas. *J. Photochem. Photobiol., A* **2004**, *163*, 69−75.

(29) Bridges, J. W.; Williams, R. T. The Fluorescence of Indoles and Aniline Derivatives. *Biochem. J.* **1968**, *107*, 225−237.

(30) McHale, J. L. *Molecular Spectroscopy*; Prentice Hall: New York, 1999.

(31) Srividya, N.; Sinha, A.; Prasada Rao, T. A. Solvent Effects on the Absorption and Emission Spectra of Some Nematic Liquid Crystals: Determination of Dipole Moment and First-Order Hyperpolarizability. *J. Sol. Chem.* **2000**, *29*, 847−857.

(32) Williams, R. T.; Bridges, J. W. Fluorescence of Solutions. A Review. *J. Clin. Pathol.* **1964**, *17*, 371−394.

(33) Birks, J. B. *Photophysics of Aromatic Molecules*; Wiley: New York, 1970.

(34) Gutavsson, L.; Cassara, V.; Gulbinas, G.; Gurzadyan, J. C.; Mialocq, S.; Pommeret, M.; Sorguis, P. M. Femtosecond Spectroscopic Study of Relaxation Processes of Three Amino-Substituted Coumarin Dyes in Methanol and Dimethyl Sulfoxide. *J. Phys. Chem. A* **1998**, *102*, 4229−4245.

(35) Saha, S. K.; Dogra, S. K. Solvatochromic Effects in the Absorption and Fluorescence Spectra of Indazole and Its Amino Derivatives. *J. Photochem. Photobiol., A* **1997**, *110*, 257−266.

(36) Köhler, G. Solvent Effects on the Fluorescence Properties of Anilines. *J. Photochem.* **1987**, *38*, 217−238.
(37) Bridges, J. W.; Gifford, L. A.; Hayes, W. P.; Miller, J. N.; Burns, D. T. Luminiscence Properties of Sulfonamide Drugs. *Anal. Chem.* **1974**, *46*, 1010−1017.
(38) Förster, T. Die $\rho_H$-Abhägigkeit der Fluoreszenz von Naphthalinderivaten. *Z. Elektrochem. Angew. Phys. Chem.* **1950**, *54*, 531−535.
(39) Jaffé, H. H.; Jones, H. L. Excited State pK Values. III. The Application of the Hammett Equation. *J. Org. Chem.* **1965**, *30*, 964−969.
(40) Venning, D. R.; Mousa, J. J.; Lukasiewicz, R. J.; Winefordner, J. D. Influence of Solvent upon the Phosphorescence Characteristics of Several Sulfonamides at 77 K. *Anal. Chem.* **1972**, *44*, 2387−2389.
(41) Tobita, S.; Ida, K.; Shiobara, S. Water-Induced Fluorescence Quenching of Aniline and Its Derivatives in Aqueous Solution. *Res. Chem. Intermed.* **2001**, *27*, 205−218.
(42) Saito, F.; Tobita, S.; Shizuka, H. Photoionization of Aniline in Aqueous Solution and its Photolysis in Cyclohexane. *J. Chem. Soc., Faraday Trans.* **1996**, *92*, 4177−4185.
(43) Forbes, W. F. The Study of Hydrogen Bonding and Related Phenomena by Ultraviolet Light Absorption 0.4. Intermolecular Hydrogen Bonding in Anilines and Phenols. *Can. J. Chem.* **1960**, *38*, 896−910.
(44) Blais, J.; Gauthier, M. Effects of Inter-Molecular Interactions by Hydrogen-Bond on Absorption and Luminescence of Aromatic-Amines in Vitreous Matrix at 77-K. *J. Photochem.* **1978**, *9*, 529−538.
(45) Strickler, S. J.; Berg, R. A. Relationship between Absorption Intensity and Fluorescence Lifetime of Molecules. *J. Chem. Phys.* **1962**, *37*, 814.
(46) Tsubomura, H.; Mulliken, R. S. Molecular Complexes and Their Spectra. XII. Ultraviolet Absorption Spectra Caused by the Interaction of Oxygen with Organic Molecules. *J. Am. Chem. Soc.* **1960**, *82*, 5966−5974.
(47) Bakhshiev, N. G. New Version of the Semiempirical Theory of the Effect of the Dielectric Properties of Individual Solvents on the Shift of the Absorption Spectra of Solutions. *J. Opt. Technol.* **2001**, *68*, 184−188.
(48) Jozefowicz, M.; Milart, P.; Heldt, J. R. Determination of Ground and Excited State Dipole Moments of 4,5′-Diamino[1,1′:3′,1″-terphenyl]-4′,6 ′-dicarbonitrile using Solvatochromic Method and Quantum-Chemical Calculations. *Spectrochim. Acta, Part A* **2009**, *74*, 959−963.
(49) Reichardt, C. *Solvents and Solvent Effects in Organic Chemistry*; Wiley-VCH: Weinheim, Germany, 2003.
(50) Suppan, P.; Ghoneim, N. *Solvatochromism*; Royal Society of Chemistry: Cambridge, U.K., 1997.
(51) Lippert, E. Dipolmoment und Elecktronenstruktur von Angeregten Molekülen. *Z. Naturforsch.* **1955**, *109*, 541−545.
(52) Lippert, E. Spektroskopische Bestimmung des Dipolmomentes aromatischer Verbindungen im ersten angeregten Singulettzustand. *Z. Elektrochem.* **1957**, *61*, 962−975.
(53) Mataga, N.; Kaifu, Y.; Koizumi, M. The Solvent Effect on Fluorescence Spectrum: Change of Solute−Solvent Interaction During the Lifetime of Excited Solute Molecule. *Bull. Chem. Soc. Jpn.* **1955**, *28*, 690−691.
(54) Mataga, N.; Kaifu, Y.; Koizumi, M. Solvent Effects upon Fluorescence Spectra and the Dipolemoments of Excited Molecules. *Bull. Chem. Soc. Jpn.* **1956**, *29*, 465−470.
(55) Rechthaler, K.; Köhler, G. Excited-State Properties and Deactivation Pathways of 7-Aminocoumarins. *Chem. Phys. Lett.* **1994**, *189*, 99−116.
(56) Ledger, M. B.; Suppan, P. Anomalous Spectroscopic Shifts and Structure of 1,4-Dioxan. *Spectrochim. Acta, Part A* **1967**, *23*, 3007−3011.
(57) Marcus, Y. The Properties of Organic Liquids that are Relevant to Their Use as Solvating Solvents. *Chem. Soc. Rev.* **1993**, *22*, 409−416.
(58) Catalán, J. In *Handbook of Solvents*; Wypych, G., Ed.; ChemTech Publishing: Toronto, Canada, 2001; Chapter 9.3, ppp 583−616.
(59) Catalán, J.; Díaz, C. A Generalized Solvent Acidity Scale: the Solvatochromism of *o*-*tert*-Butylstilbazolium Betaine Dye and its Homomorph *o*,*o*′-di-*tert*-Butylstilbazolium Betaine Dye. *Liebigs Ann./Recl.* **1997**, 1941−1949.
(60) Catalán, J.; Díaz, C.; López, V.; Pérez, P.; de Paz, J. L. G.; Rodríguez, J. G. A Generalized Solvent Basicity Scale: the Solvatochromism of 5-Nitroindoline and Its Homomorph 1-Methyl-5-nitroindoline. *Liebigs Ann./Recl.* **1996**, *11*, 1785−1794.
(61) Catalán, J.; Hopf, H. Empirical Treatment of ohe Inductive and Dispersive Components of Solute−Solvent Interactions: the Solvent Polarizability (SP) Scale. *Eur. J. Org. Chem.* **2004**, *22*, 4694−4702.
(62) Catalán, J. Toward a Generalized Treatment of the Solvent Effect Based on Four Empirical Scales: Dipolarity (SdP, a New Scale), Polarizability (SP), Acidity (SA), and Basicity (SB) of the Medium. *J. Phys. Chem. B* **2009**, *113*, 5951−5960.
(63) Ferretti, V.; Bertolasi, V.; Cilli, P.; Cilli, C. Out-of-Plane Deformation Pathways of the R(X═)C−NR2 Fragment Present in Amides, Thioamides, Amidines, Enamines, and Anilines. A Concerted Study Making Use of Structural Data, Molecular Mechanics, and ab Initio Calculations. *J. Phys. Chem.* **1993**, *97*, 13568−13574.
(64) Platt, J. R. Classification of Spectra of Cata-Condensed Hydrocarbons. *J. Chem. Phys.* **1949**, *17*, 484−495.
(65) Lower, S. K.; El-Sayed, M. A. Triplet State and Molecular Electronic Processes in Organic Molecules. *Chem. Rev.* **1966**, *66*, 199−241.
(66) Evans, D. G.; Boeyens, J. C. A. Conformational-Analysis of Ring Rucker. *Acta Crystallogr., Sect. B: Struct. Sci.* **1989**, *45*, 581−590.
(67) Palmer, I. J.; Ragazos, I. N.; Bemardi, F.; Olivucci, M.; Robb, M. A. An MC-SCF Study of the S1 and S2 Photochemical-Reactions of Benzene. *J. Am. Chem. Soc.* **1993**, *115*, 673−682.
(68) Rubio-Pons, O.; Serrano-Andrés, L.; Merchán, M. A Theoretical Insight into the Photophysics of Acridine. *J. Phys. Chem. A* **2001**, *105*, 9664−9673.
(69) Tatchen, J.; Gilka, N.; Marian, C. M. Intersystem Crossing Driven by Vibronic Spin-Orbit Coupling: a Case Study on Psoralen. *Phys. Chem. Chem. Phys.* **2007**, *9*, 5209−5221.
(70) Climent, T.; González-Luque, R.; Merchán, M.; Serrano-Andrés, L. On the Intrinsic Population of the Lowest Triplet State of Uracil. *Chem. Phys. Lett.* **2007**, *441*, 327−331.
(71) Serrano-Pérez, J. J.; González-Luque, R.; Merchán, M.; Serrano-Andrés, L. On the Intrinsic Population of the Lowest Triplet State of Thymine. *J. Phys. Chem. B* **2007**, *111*, 11880−11883.
(72) Bazyl, O. K.; Chaikovskaya, O. N.; Artyukhov, V. Y. The Effect of Complexation on the Spectral and Luminescent Properties and Photolysis of Methyl[(4-aminophenyl)sulfonyl] Carbamate. *Opt. Spectrosc.* **2005**, *98*, 838−843.
(73) Bazyl, O. K.; Chaikovskaya, O. N.; Artyukhov, V. Y.; Maier, G. V. A Quantum-Chemical Study of the Spectral and Luminescent Properties and Photolysis of Methyl[(4-aminophenyl) sulfonyl] Carbamate. *Opt. Spectrosc.* **2004**, *97*, 42−47.